

CAPER: Constrained and Procedural Reasoning for Robotic Scientific Experiments

Jinghan Yang¹, Jingyi Hou^{1*}, Xinbo Yu¹ and Wei He^{1,2} and Yifan Wu¹

¹University of Science and Technology Beijing

²Beijing Information Science and Technology University

*houjingyi@ustb.edu.cn

Abstract

Robotic assistance in scientific laboratories requires procedurally correct long-horizon manipulation, reliable execution under limited supervision, and robustness in low-demonstration regimes. Such conditions greatly challenge end-to-end vision-language-action (VLA) models, whose assumptions of recoverable errors and data-driven policy learning often break down in protocol-sensitive experiments. We propose CAPER, a framework for Constrained And Procedural Reasoning for robotic scientific experiments, which explicitly restricts where learning and reasoning occur in the planning and control pipeline. Rather than strengthening end-to-end policies, CAPER enforces a responsibility-separated structure: task-level reasoning generates procedurally valid action sequences under explicit constraints, mid-level multimodal grounding realizes subtasks without delegating spatial decision-making to large language models, and low-level control adapts to physical uncertainty via reinforcement learning with minimal demonstrations. By encoding procedural commitments through interpretable intermediate representations, CAPER prevents execution-time violations of experimental logic, improving controllability, robustness, and data efficiency. Experiments on a scientific workflow benchmark and a public long-horizon manipulation dataset demonstrate consistent improvements in success rate and procedural correctness, particularly in low-data and long-horizon settings.

1 Introduction

Robotic assistance in scientific laboratories aims to support researchers during the research-and-development (R&D) stage by offloading repetitive and time-consuming experimental procedures, such as material synthesis, chemical preparation, and standardized testing. While recent systems have demonstrated reliable automation in highly structured and fully specified laboratory pipelines [Pyzer-Knapp *et al.*, 2022; Wang and Zhu, 2024; Ramos *et al.*, 2025], real-world R&D experiments impose requirements that fundamentally

differ from those of routine or closed-form automation. Scientists often specify only high-level experimental goals, leaving critical procedural details (e.g., step ordering, prerequisite conditions, and irreversible operations) underspecified. As a result, success in scientific experimentation is determined not merely by task completion, but by strict adherence to experimental protocols. Moreover, experimental workflows in R&D settings are often executed under limited supervision, with sparse, weak, or biased demonstrations that reflect procedural conventions rather than action trajectories. These characteristics make long-horizon robotic manipulation in scientific laboratories uniquely challenging, demanding procedural correctness, robustness under weak supervision, and reliability over extended action sequences.

Recent advances in large language models (LLMs) have demonstrated strong capabilities in task decomposition and logical reasoning [Ha *et al.*, 2023; Dalal *et al.*, 2024; Zhou *et al.*, 2024; Guo *et al.*, 2024], while vision-language-action (VLA) models [Ma *et al.*, 2024; Black *et al.*, 2025; Zhao *et al.*, 2025] attempt to unify perception and reasoning in an end-to-end manner. Despite their success on household and industrial benchmarks, these methods might face limitations in aligning with R&D-stage scientific experimentation. End-to-end VLAs implicitly rely on the recoverability of execution errors, dense trajectory supervision, and the ability to absorb task logic into latent action representations. In scientific experiments, these assumptions break down, as errors are often irreversible and procedural validity cannot be learned reliably from sparse demonstrations. As task horizons grow and experimental procedures become compositional, the space of valid action sequences expands combinatorially, making purely data-driven generalization expensive. This limitation echoes broader findings on systematic generalization [Lake and Baroni, 2018; Bahdanau *et al.*, 2019], and is further exacerbated by recent evidence that task-specific fine-tuning of VLA models can bias policies toward superficial goal completion while neglecting underlying state and protocol correctness [Li *et al.*, 2024]. Together, these observations suggest that the challenges faced by end-to-end VLA models in scientific domains are not incidental, but structural. Such evidence reveals the inherent shortcomings of purely end-to-end learning in robotic scientific experiments.

These limitations suggest rethinking how learning and reasoning are structured in long-horizon robotic manipulation

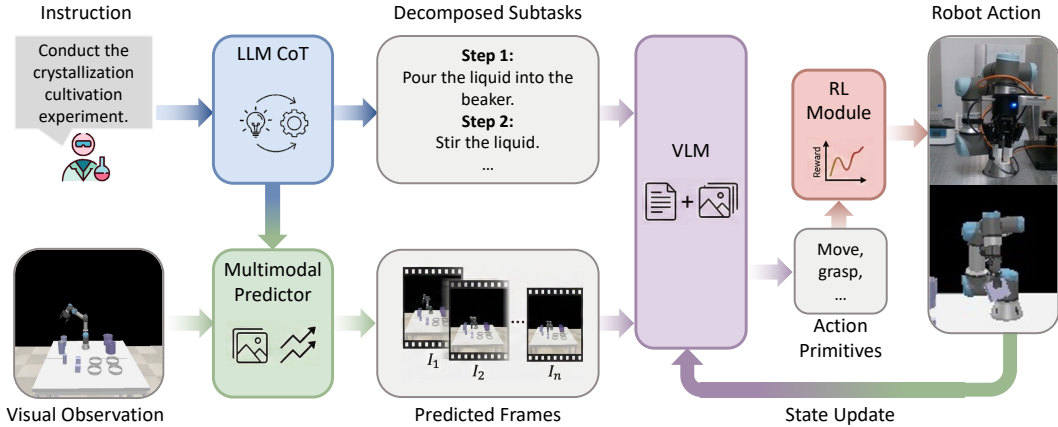


Figure 1: Overview of the CAPER framework. CAPER decomposes long-horizon tasks into modular stages. First, an LLM generates procedurally valid sequence of high-level subtasks in symbolic space, without access to visual or control signals. A multimodal planner, composed of a multimodal predictor and a VLM, then grounds each subtask by conditioning on the current and predicted goal images, producing sequences of action primitives. Finally, a low-level controller executes these primitives in the environment, enabling safe and consistent task completion.

for scientific R&D experiments. Rather than strengthening end-to-end policies, learning and reasoning should be explicitly constrained. In scientific workflows, procedural logic and perceptual uncertainty often arise at different levels. Deferring procedural reasoning to latent action representations couples these factors, complicating error analysis and corrective intervention. Instead, procedural reasoning should be treated as an explicit commitment made prior to execution, narrowing the space of admissible actions and shielding downstream modules from semantic ambiguity. Instead, making procedural reasoning explicit prior to execution allows the action space to be constrained in advance, reducing ambiguity during downstream execution. Motivated by this observation, we propose CAPER (Constrained And ProcEdural Reasoning) for robotic Scientific Experiments, a framework that enforces a responsibility-separated structure across task-level reasoning, mid-level grounding, and low-level control. By explicitly encoding procedural commitments through interpretable intermediate representations, CAPER prevents execution-time violations of experimental logic and enables each component to focus on the uncertainties it is best suited to handle.

Specifically, CAPER organizes long-horizon robotic manipulation into three decoupled stages that reflect the structure of scientific workflows. Task-level reasoning procedurally valid action sequences under explicit constraints, resolving ordering and prerequisite relations before conduct. Mid-level grounding realizes each subtask through multimodal perception without delegating spatial decision-making to LLMs. Low-level control then adapts execution to physical uncertainty through reinforcement learning, without relying on explicit trajectory supervision. This responsibility-separated design allows procedural logic, perceptual grounding, and physical control to be handled at appropriate levels of abstraction. We evaluate CAPER on a scientific workflow benchmark designed to emphasize procedural validity, as well as on a public long-horizon manipulation dataset.

Across both settings, CAPER achieves consistent improvements in task success and procedural correctness, with particularly strong gains in low-data and long-horizon regimes.

2 Related Work

Robot manipulation learning Robotic manipulation has traditionally relied on symbolic planning and control methods such as trajectory optimization [Parr and Russell, 1997; Kaelbling and Lozano-Pérez, 2011], which work well in structured settings but lack flexibility and generalization. Recent advances in LLMs [Radford, 2018; Touvron *et al.*, 2023] have inspired their use in robotic skill learning [Ichter *et al.*, 2022], programmatic task decomposition [Singh *et al.*, 2023], and in combination with RL for low-level control [Datal *et al.*, 2024], though these approaches are often limited by unstable execution and poor systematic generalization. VLA models aim to unify perception, reasoning, and control [Yu *et al.*, 2025; Sautenkov *et al.*, 2025; Zhang *et al.*, 2025], but purely end-to-end training struggles to scale as task compositions grow combinatorially, since task-level constraints and procedural dependencies must be implicitly absorbed into action distributions. CoT-VLA [Zhao *et al.*, 2025] and HAMSTER [Li *et al.*, 2025] move toward hierarchical structures by incorporating CoT reasoning or coarse-to-fine path planning, yet they remain tightly coupled through trajectory-level supervision, where intermediate reasoning and execution are co-adapted rather than independently optimized. In contrast, our proposed CAPER explicitly disentangles task decomposition, multimodal prediction, and low-level control into heterogeneous modules. This modularity allows independent optimization without trajectory-level supervision, enabling controllable procedural reasoning and robust compositional recombination under domain shifts.

Autonomous experimental systems for science Prior works have focused on autonomous scientific discovery by

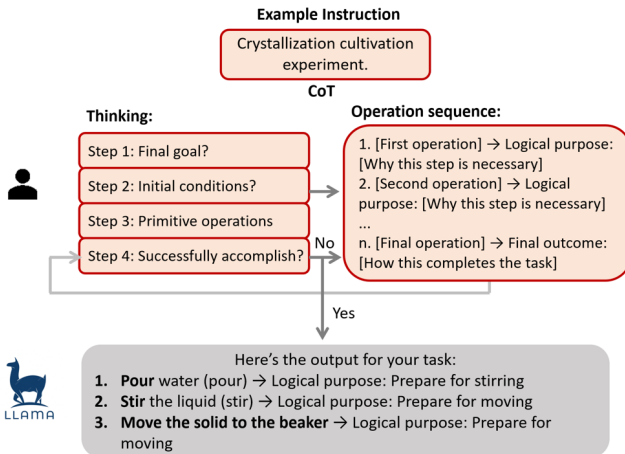


Figure 2: An example of the task-level planner using CoT reasoning. The LLM is guided through a 4-step process: (1) clarify the goal, (2) identify required objects and conditions, (3) decompose into basic operations, and (4) validate task completion.

combining high-throughput experimentation and AI-driven planning. For example, [Zhao *et al.*, 2021] leverage automated platforms to explore the stability of perovskites under varying conditions. [Coley *et al.*, 2019] develop an organic synthesis platform using robotic arms and modular components to automate complex chemical processes. [Burger *et al.*, 2020] propose a mobile chemical robot that performs hundreds of experiments autonomously to discover a novel hydrogen-production catalyst. These systems typically assume tightly integrated, domain-specific platforms and pre-defined experimental pipelines, limiting their flexibility for open-ended laboratory workflows. Our work focuses instead on experimental assistance during the R&D process to help researchers perform tedious lab tasks more efficiently.

3 Method

3.1 Pipeline overview

Long-horizon robotic planning requires reasoning, visual grounding, and reliable skill execution, which are challenging to achieve within a single end-to-end model. To address this, we introduce a constrained and procedural reasoning framework (CAPER) that disentangles these stages (Fig. 1).

3.2 Task-level planner

We model the task-level planner as a symbolic decomposition process, operating entirely in the language space and decoupled from perception or control signals. As shown in Fig. 2, given a high-level goal G (e.g., “crystallization cultivation experiment.”), we use CoT reasoning with the Meta-Llama-3.1-8B-Instruct model to generate a sequence of semantically coherent subtasks

$$\mathcal{S} = \{s_1, s_2, \dots, s_T\}, \quad s_t \in \mathcal{L}, \quad (1)$$

where \mathcal{L} denotes the symbolic instruction space (natural-language actions such as “add reagent A”).

To construct \mathcal{S} , we employ CoT prompting, which decomposes reasoning into four stages:

$$G \xrightarrow{(1) \text{ interpret}} g \xrightarrow{(2) \text{ prerequisites}} \mathcal{P} \xrightarrow{(3) \text{ decompose}} \mathcal{S} \xrightarrow{(4) \text{ validate}} \mathcal{S}^*,$$

where g denotes the interpreted core objective, \mathcal{P} is the set of prerequisite conditions, and \mathcal{S}^* is the optimized subtask sequence after logical validation.

To improve reliability, we introduce a verification-correction loop applied iteratively:

$$\mathcal{S}^{(k+1)} = \Phi(\mathcal{S}^{(k)}), \quad \Phi = f_{\text{val}} \circ f_{\text{cons}} \circ f_{\text{corr}}, \quad (2)$$

where f_{val} performs subgoal validation, f_{cons} checks temporal/causal/physical constraints, and f_{corr} applies corrections (see detailed description in Appendix B). This process continues until $\mathcal{S}^{(k)}$ converges to a logically consistent plan \mathcal{S}^* . This mechanism operates entirely within the LLM without external labels, leveraging its inherent reasoning abilities to ensure semantic correctness. As the task-level planner is performed in the symbolic space of language, it is decoupled from direct visual inputs.

The output \mathcal{S}^* resides purely in the symbolic language space and is therefore independent of low-level visual observations. Formally, we define a two-stage factorization of the overall policy:

$$\pi(a_t | o_t, G) = \pi_{\text{exec}}(a_t | o_t, \mathcal{S}^*), \quad \mathcal{S}^* = \pi_{\text{plan}}(G), \quad (3)$$

where π_{plan} maps high-level goals G into symbolic plans, and π_{exec} grounds these symbolic subtasks into action primitives a_t conditioned on visual observations o_t , which will be described in detail in the following section w.r.t the multimodal planner.

This factorization highlights the modularity of our framework: the task-level planner is responsible for semantic reasoning in symbolic space, while mid-level multimodal planner and low-level controller modules handle grounding and execution. Such a separation improves robustness and reusability, especially in complex, sensor-rich scientific environments. We provide a detailed discussion on the feasibility of the decoupling manner in Appendix C.

3.3 Mid-level multimodal planner

The mid-level multimodal planner bridges high-level task decomposition and low-level control by grounding each subtask in perceptual observations. It consists of two components: (1) a multimodal predictor that provides execution-relevant visual context by predicting future scene states, and (2) a VLM that maps grounded subtasks to structured action primitives that can be executed by the controller.

Visual prediction

The multimodal predictor is based on a conditional diffusion model [Du *et al.*, 2023] and is used to estimate short-horizon future visual states during subtask execution. Given the current observation and a subtask description, the model predicts a sequence of intermediate frames that reflect how the scene is likely to evolve if the subtask is carried out. These predicted frames are not used to choose actions, but to provide visual context that supports grounding and execution.

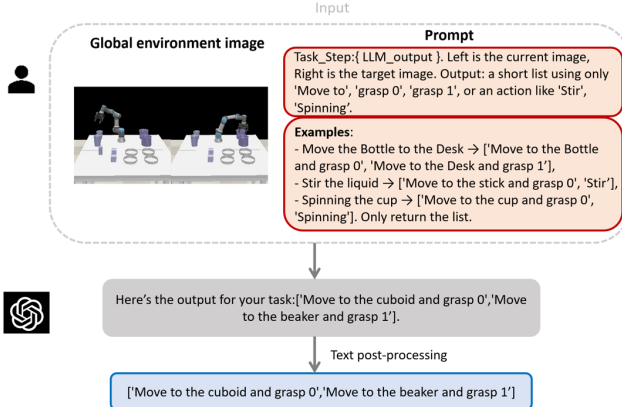


Figure 3: An example prompt used for the VLM.

Task instructions are encoded by a frozen CLIP encoder, while a UNet backbone extracts visual features from the current frame. We fuse the two streams via cross-attention, so the predictor conditions on both the scene and the subtask semantics.

We use a conditional diffusion formulation. Let x_0 denote the clean future frame (or a future-frame sequence element) and x_t the noisy sample at diffusion step t . The forward noising process is

$$q(x_t | x_{t-1}) = \mathcal{N}\left(x_t; \sqrt{1 - \beta_t} x_{t-1}, \beta_t \mathbf{I}\right), \quad (4)$$

with a predefined noise schedule $\{\beta_t\}_{t=1}^T$. In the reverse process, the model predicts the noise and denoises step-by-step:

$$x_{t-1} = \frac{1}{\sqrt{1 - \beta_t}} \left(x_t - \frac{\beta_t}{\sqrt{1 - \bar{\alpha}_t}} \epsilon_\theta(x_t, t) \right) + \sigma_t z, \quad (5)$$

where $z \sim \mathcal{N}(0, \mathbf{I})$ and ϵ_θ is parameterized by a UNet conditioned on the current observation and the CLIP embedding.

Given the current frame i_0 and subtask text l , the predictor outputs a short sequence of future frames

$$P_\theta(i_0, l) \rightarrow \{\hat{i}_1, \hat{i}_2, \dots, \hat{i}_K\}, \quad (6)$$

which provides visual context for grounding. We train the predictor with the standard noise-prediction objective and apply SNR-based reweighting [Ho *et al.*, 2020] and use gradient clipping for stability.

For scientific experiment scenes, we train on trajectories collected in a simulated laboratory environment. We crop low-information regions, use 256×256 inputs, and sample $K=8$ frames per sequence. By predicting likely future configurations, the model helps expose spatial conflicts (e.g., potential collisions) and improves the robustness of downstream grounding and execution.

Action primitive generation

Given a symbolic subtask and visual observations, we convert the subtask into a sequence of executable action primitives. We use a vision-language model (GPT-4o) to map each subtask to a small set of predefined action primitives commonly used in laboratory settings: `move`, `grasp`, `pour`, and

`stir`. To reduce ambiguity, we adopt a structured prompt format (Fig. 3) that conditions the VLM on paired visual inputs (the current observation and a predicted future frame) together with the subtask description.

Most subtasks are realized through combinations of `move` and `grasp`, with sequential execution represented by simple concatenation (e.g., “`move` and `grasp`”). Operations such as `pour` and `stir` are treated as atomic actions and are invoked directly when required. Each `move` primitive is expressed as `move to <target>`, and each `grasp` as `grasp 1/0`, indicating grasp or release.

The VLM outputs a structured sequence of action primitives that serves as an interpretable and robot-compatible intermediate representation. This representation provides a simple interface to the low-level controller and supports downstream reinforcement learning, where execution policies are refined through interaction with the environment.

3.4 Low-level controller

Recent diffusion-based and ACT-based VLAs show strong trajectory generation ability, but often suffer from fragile visual grounding when perception is implicitly coupled with action generation. In end-to-end formulations, grounding errors directly translate into execution failures and repeated attempts, without an explicit interface for inspection or correction. CAPER avoids this issue by resolving task reasoning and visual grounding upstream, and restricting the low-level controller to executing fixed action primitives.

To execute the action primitives, we use a continuous-control policy that maps observations to joint-level commands. While DDPG [Lillicrap *et al.*, 2016] is one possible choice, other continuous controllers can be used. Reinforcement learning is applied only at this level to improve primitive execution under local feedback, without reintroducing perceptual or task-level uncertainty.

The reward function balances task progress, success, and safety:

$$r = r_{\text{move}} + r_{\text{grasp}} - r_{\text{collision}}, \quad (7)$$

where r_{move} encourages approaching the target, r_{grasp} rewards successful grasps, and $r_{\text{collision}}$ penalizes collisions.

To support long-horizon tasks, the environment is reset only at task initialization or completion, maintaining continuity across subtasks.

3.5 Simulation setup

We build the simulation environment using CoppeliaSim (V-REP), designed for scientific experimental scenarios. A UR3 robotic arm is used as the execution platform. The environment includes common laboratory apparatus such as beakers and Petri dishes, as well as graspable objects including cylinders, cubes, cups, and sticks, which abstract different categories of experimental items.

The simulator provides collision detection and distance sensing. Low-level controllers can access object states through the environment interface to compute rewards during training. Based on this environment, we collect a dataset for scientific manipulation tasks, covering both long-horizon and extra-long-horizon experimental procedures. Instead of

Table 1: Training tasks and prompt templates of the scientific experiment dataset.

Task	Description	Prompt template	Environment	#Training data
Pick_place	Basic object relocation.	1. Move <object> to <object>. 2. Put <object> on <object>. 3. Place <object> next to <object>. ...	Simulation	88
Pour	Single-step pouring of liquid.	1. Pour <liquid>. 2. Pour <liquid> into <container>. 3. Pour <liquid> from <container>. ...	Simulation	25
Stir	Stir the liquid in a container.	1. Stir <liquid>. 2. Stir <liquid> in <container>. 3. Perform stirring. ...	Simulation	27
Mix	Multi-step reactant mixing experiment.	1. Conduct reactant mixing experiment. 2. Perform multi-step mixing. 3. Combine <liquid> and <liquid>. ...	Simulation	50
Crystallize	Crystallization cultivation experiment.	1. Conduct crystallization. 2. Grow <object> from <solution>. 3. Perform crystallization cultivation. ...	Simulation	73
Weigh	Weigh the liquid content within the container.	1. Weigh <object>. 2. Weigh <object> with the balance. ...	Real-world	27
Shake	Load the container onto the shaker.	1. Load <container> onto the shaker. 2. Shake <container>. ...	Real-world	25

assigning a single fixed instruction to each task, we construct a pool of prompt templates for every task category. Each pool contains semantically equivalent but lexically diverse instructions generated by an LLM, increasing linguistic variability while preserving task intent.

The dataset includes tasks such as object relocation, pouring, stirring, multi-step reactant mixing, and crystallization cultivation. For each task instance, the dataset records the execution trajectories required to complete the target procedure. The number of training samples for each task is summarized in Table 1. This dataset is sufficient for training the multimodal predictor to produce stable and accurate visual predictions.

For the evaluation of each task, multiple instructions are sampled from the corresponding prompt-template pool and paired with different object combinations to form 20 distinct input prompts. For each prompt, we further sample 50 randomized initial scenes with varying object poses and spatial layouts, resulting in 1,000 evaluation trials per task.

4 Experiments

4.1 Experimental setup

All experiments are conducted on a single NVIDIA GeForce RTX 4090 GPU for both training and inference. Due to GPU memory constraints, we use a batch size of 1, where each batch contains 8 consecutive robot motion frames from a single task instance. All input images are resized to a resolution of 256×256 . For low-level control, we employ DDPG, with a replay buffer size of 4.

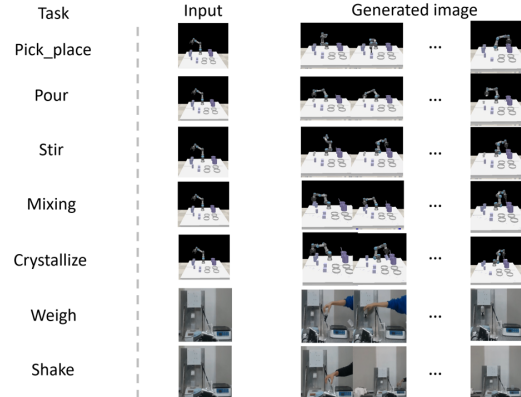


Figure 4: Examples of predicted future visual frames generated by the multimodal predictor under different task conditions.

4.2 Visualization

To evaluate the quality of future frames generated by the multimodal predictor, we measure both visual clarity and semantic alignment using standard quantitative metrics:

Laplacian Variance is used to quantify image sharpness by computing the variance of the Laplacian response for each predicted frame.

CLIP Similarity quantifies the semantic alignment between task instructions and predicted images. We extract embeddings using a pretrained CLIP model and compute cosine similarity between the instruction text and the corresponding predicted frames.

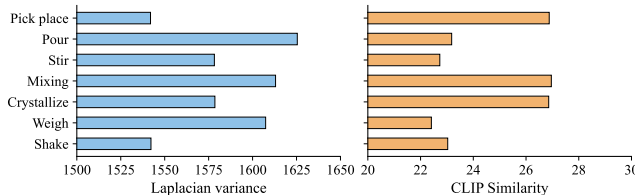


Figure 5: Visual clarity and semantic relevance of predicted images.

Results are shown in Fig. 5. The predicted frames consistently achieve Laplacian variance values above 1,500, indicating sufficient visual sharpness to preserve motion boundaries and object contours. In addition, CLIP similarity scores remain above 21, suggesting strong semantic alignment between task descriptions and predicted visual content. Such alignment supports stable subtask grounding by providing task-consistent visual context.

Examples of predicted future frames for different tasks are shown in Fig. 4.

4.3 Experimental results on the scientific experiment dataset (simulation)

We test the success rates of CAPER and other methods using the benchmark we designed. In approaches that only rely on RL model, the DDPG model exhibits near-zero success rates on complex, long-horizon tasks due to the absence of task decomposition and planning mechanisms. Its performance is nearly indistinguishable from random trial-and-error, making meaningful comparison infeasible. The success rates of different methods are shown in Table 2.

LLM+RL (LLaMA-3.1-8B, w/o CoT). We remove the multimodal predictor (MP) and replace the mid-level VLM with LLaMA-3.1-8B, without CoT prompting. Subtasks are generated directly from textual task and environment descriptions and executed by the RL controller. This baseline evaluates the limitation of language-only task decomposition without visual grounding or structured reasoning.

VLM+RL (LLaMA3.2, w/o CoT). We introduce visual input by replacing the LLM with a VLM. This setting evaluates the contribution of visual information to task decomposition in the absence of CoT reasoning.

LLM+RL (GPT-4o). We use GPT-4o with CoT prompting for task decomposition, but without visual input. This baseline isolates the effect of strong language reasoning without visual grounding.

VLM+RL (GPT-4o). We remove both the multimodal predictor and the task-level planner from CAPER, relying on a VLM to generate subtasks directly from visual observations. Compared with the LLaMA3.2-based VLM+RL baseline, this setting highlights the effectiveness of our structured prompting, while the performance drop indicates the importance of explicit grounding and planning.

MP+VLM+RL (GPT-4o). We remove only the task-level planner from CAPER to assess its role. Performance differences are minor for short-horizon tasks, but become pronounced for long-horizon tasks such as mixing and crystallize, demonstrating the necessity of explicit task-level plan-

ning.

CAPER. CAPER achieves the best overall performance on the scientific experiment benchmark. It performs strongly on relatively short-horizon tasks such as pick_place, while showing a moderate performance drop on pour and stir, primarily due to grasp instability caused by thin tools and challenging end-effector poses, which increase the likelihood of slippage during execution. For long-horizon tasks including mixing and crystallize, success rates decrease further as visual ambiguity and procedural complexity accumulate over time. Nevertheless, CAPER consistently outperforms all baselines, demonstrating the necessity and effectiveness of integrating task-level planning, explicit grounding, and learned execution.

From the experimental results, we observe the critical role of visual information and CoT reasoning structure within the CAPER framework. Moreover, each module in CAPER proves to be indispensable. The success rate of CAPER in scientific experiment tasks meets the practical requirements of such experiments.

4.4 Experimental results on the scientific experiment dataset (real-world)

We design a sim-to-real setup where real-world objects differ in shape from simulation but share the same sizes and spatial layouts. Object poses are obtained using a D415 depth camera with YOLOv8 and mapped to the simulation frame.

For real-world evaluation, we conduct 40 trials each on the tasks Pick_place, Pour, and Stir, 20 trials on the extra-long-horizon tasks Mixing and Crystallize, and 10 trials on the real-only tasks Weigh and Shake. CAPER achieves success rates of 75.0%, 62.5%, 70.0%, 50.0%, 25.0%, 70.0%, and 70.0% on these tasks, respectively.

As shown in Fig. 6, the performance gap between simulation and real-world execution remains moderate. Importantly, the observed drop is mainly caused by inaccuracies in object detection and depth estimation, rather than limitations of task reasoning or execution. Such errors are confined to the perception module and can be mitigated by improving sensing accuracy, without retraining the task-level planner or the low-level controller. Notably, the Weigh and Shake tasks are executed purely in real-world settings, without any corresponding simulation environment. These tasks are performed using the same action primitives and execution policies learned in simulation, without additional RL training. This result indicates that CAPER supports direct deployment in real-world scenarios where simulation is unavailable, by decoupling procedural structure and execution from environment-specific perception. Further analysis is provided in Appendix.

4.5 Experimental results on the public dataset

We further evaluate CAPER on RLBench [James *et al.*, 2020], a widely used robotic manipulation benchmark. To differentiate CAPER from CoT-VLA, and owing that the code of CoT-VLA is not publicly available, we reproduced the entire pipeline based on the VILA-U model [Wu *et al.*, 2025] described in the CoT-VLA paper. To ensure a fair comparison, all models are trained on the same task-specific training data without pretraining on real-world demonstrations or

Task	LLM+RL (Llama-3.1-8B w/o CoT)	MLM+RL (LLaMA3.2 w/o CoT)	LLM+RL (GPT-4o)	MLM+RL (GPT-4o)	MP+MLM+RL (GPT-4o)	CAPER
Pick_place	39.6	45.8	70.4	78.9	79.3	80.3
Pour	34.8	44.7	54.6	62.6	62.4	64.5
Stir	30.2	39.6	34.8	70.5	70.8	74.4
Mix	23.3	35.5	23.8	43.2	43.6	52.3
Crystallize	11.6	12.9	12.4	21.0	21.5	30.1

Table 2: Success rate (%) of different methods on the scientific experiment dataset.

Task	PerAct	OpenVLA	CoT-VLA [*]	MoLe-CogAct	CAPER
Pick cup	40.0	84.0	86.0	85.2	48.0
Push button	48.0	82.4	84.0	88.0	80.0
Take umbrella	20.0	28.0	32.0	36.0	42.4
Put knife	16.0	8.0	10.4	26.4	73.2
Put money	44.0	22.4	24.0	30.0	46.4

^{*}Re-implemented following the paper, as official code is unavailable.

Table 3: Success rate (%) of different methods on RLBench.

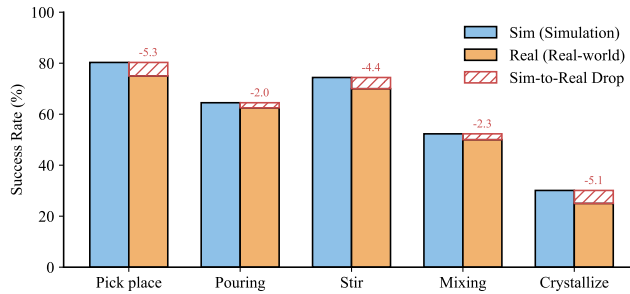


Figure 6: Sim-to-real performance comparison & drop analysis.

action-free videos, which may negatively impact performance in simulation.

We select 5 long-horizon tasks that closely align with the typical procedures of scientific experiments in RLBench to validate the performance of CAPER, and compare the success rate with PerAct [Shridhar *et al.*, 2022], OpenVLA [Kim *et al.*, 2024], CoT-VLA [Zhao *et al.*, 2025] and MoLe-CogAct [Zhang *et al.*, 2025] methods. We evaluate the success rates of CAPER and other methods using the benchmark we developed, presenting the average success rate across 3 evaluation rounds, each with 25 trials. As shown in Table 3, CAPER achieves the highest success rates on long-horizon tasks, demonstrating stronger robustness and adaptability to procedural task variations. We note that performance on the pick cup task is lower than on other tasks, primarily due to a conservative grasping constraint inherited from the scientific experiment setting, where the RL controller is restricted to grasping only one side of the cup wall for safety.

4.6 Model efficiency and runtime

Most components of CAPER do not require training. All LLM and VLM modules are used off-the-shelf, while only the multimodal predictor and the RL controller are trained.

Component	Latency (ms)	RunsOnline?
LLM	3024	No
MP	5714	Optional
VLM	3441	Optional
RL	15	Yes
Online total	15	-

Table 4: Per-module inference latency and online/offline execution.

Among them, the multimodal predictor is the most computationally expensive component, whereas the RL policy can be trained on a single consumer-grade GPU (e.g., RTX 4060). Inference latency of each module is reported in Table 4.

To assess whether CAPER can be executed more efficiently, we additionally evaluate a reduced resolution of 128×128 (inference cost 978ms). We observe comparable performance under the reduced resolution, indicating that CAPER can be accelerated without significant loss of effectiveness. Details are provided in Appendix.

5 Conclusion

We presented CAPER, a framework for robotic assistance in scientific R&D laboratories that emphasizes explicit procedural structure and responsibility separation in long-horizon manipulation. By structuring task-level reasoning, perceptual grounding, and low-level control into components with well-defined roles, CAPER addresses a key mismatch between end-to-end VLAs and the requirements of protocol-sensitive experimentation. Experiments on a scientific workflow benchmark and a public long-horizon manipulation dataset show that CAPER improves robustness and procedural correctness, particularly in low-data and long-horizon settings. These results suggest that explicitly constraining where reasoning occurs can lead to more reliable and controllable robotic execution in scientific workflows.

References

Dzmitry Bahdanau, Shikhar Murty, Michael Noukhovitch, Thien Huu Nguyen, Harm de Vries, and Aaron C. Courville. Systematic generalization: What is required and can it be learned? In *ICLR*, 2019.

Kevin Black, Noah Brown, James Darpinian, Karan Dhabalia, Danny Driess, Adnan Esmail, Michael Equi, Chelsea Finn, Niccolò Fusai, et al. $\pi_{0.5}$: a vision-language-action model with open-world generalization. arXiv:2504.16054, 2025.

Benjamin Burger, Phillip M Maffettone, Vladimir V Gusev, Catherine M Aitchison, Yang Bai, Xiaoyan Wang, Xiaobo Li, Ben M Alston, Buyi Li, Rob Clowes, et al. A mobile robotic chemist. *Nature*, 583(7815):237–241, 2020.

Connor W Coley, Dale A Thomas III, Justin AM Lummiss, Jonathan N Jaworski, Christopher P Breen, Victor Schultz, Travis Hart, Joshua S Fishman, Luke Rogers, Hanyu Gao, et al. A robotic platform for flow synthesis of organic compounds informed by AI planning. *Science*, 365(6453):eaax1566, 2019.

Murtaza Dalal, Tarun Chiruvolu, Devendra Singh Chaplot, and Ruslan Salakhutdinov. Plan-seq-learn: Language model guided RL for solving long horizon robotics tasks. In *ICLR*, 2024.

Yilun Du, Sherry Yang, Bo Dai, Hanjun Dai, Ofir Nachum, Josh Tenenbaum, Dale Schuurmans, and Pieter Abbeel. Learning universal policies via text-guided video generation. In *NeurIPS*, 2023.

Weihang Guo, Zachary Kingston, and Lydia E Kavraki. CaStL: Constraints as specifications through llm translation for long-horizon task and motion planning. arXiv:2410.22225, 2024.

Huy Ha, Pete Florence, and Shuran Song. Scaling up and distilling down: Language-guided robot skill acquisition. In *CoRL*, volume 229, pages 3766–3777, 2023.

Jonathan Ho, Ajay Jain, and Pieter Abbeel. Denoising diffusion probabilistic models. In *NeurIPS*, 2020.

Brian Ichter, Anthony Brohan, Yevgen Chebotar, Chelsea Finn, Karol Hausman, Alexander Herzog, Daniel Ho, Julian Ibarz, Alex Irpan, Eric Jang, Ryan Julian, Dmitry Kalashnikov, Sergey Levine, Yao Lu, Carolina Parada, Kanishka Rao, Pierre Sermanet, Alexander Toshev, Vincent Vanhoucke, Fei Xia, Ted Xiao, Peng Xu, Mengyuan Yan, Noah Brown, Michael Ahn, Omar Cortes, Nicolas Sievers, Clayton Tan, Sichun Xu, Diego Reyes, Jarek Rettinghouse, Jornell Quiambao, Peter Pastor, Linda Luu, Kuang-Huei Lee, Yuheng Kuang, Sally Jesmonth, Nikhil J. Joshi, Kyle Jeffrey, Rosario Jauregui Ruano, Jasmine Hsu, Keerthana Gopalakrishnan, Byron David, Andy Zeng, and Chuyuan Kelly Fu. Do as I can, not as I say: Grounding language in robotic affordances. In *CoRL*, volume 205, pages 287–318, 2022.

Stephen James, Zicong Ma, David Rovick Arrojo, and Andrew J Davison. Rlbench: The robot learning benchmark & learning environment. *IEEE Robotics and Automation Letters*, 5(2):3019–3026, 2020.

Leslie Pack Kaelbling and Tomás Lozano-Pérez. Hierarchical task and motion planning in the now. In *ICRA*, pages 1470–1477, 2011.

Leslie Pack Kaelbling, Michael L. Littman, and Anthony R. Cassandra. Planning and acting in partially observable stochastic domains. *Artifical Intelligence*, 101(1-2):99–134, 1998.

Moo Jin Kim, Karl Pertsch, Siddharth Karamcheti, Ted Xiao, Ashwin Balakrishna, Suraj Nair, Rafael Rafailov, Ethan Paul Foster, Pannag R. Sanketi, Quan Vuong, Thomas Kollar, Benjamin Burchfiel, Russ Tedrake, Dorsa Sadigh, Sergey Levine, Percy Liang, and Chelsea Finn. OpenVLA: An open-source vision-language-action model. In *CoRL*, volume 270, pages 2679–2713, 2024.

Brenden M. Lake and Marco Baroni. Generalization without systematicity: On the compositional skills of sequence-to-sequence recurrent networks. In *ICML*, volume 80, pages 2879–2888, 2018.

Zichao Li, Yanshuai Cao, and Jackie CK Cheung. Do llms build world representations? probing through the lens of state abstraction. In *NeurIPS*, 2024.

Yi Li, Yuquan Deng, Jesse Zhang, Joel Jang, Marius Memmel, Caelan Reed Garrett, Fabio Ramos, Dieter Fox, Anqi Li, Abhishek Gupta, and Ankit Goyal. HAMSTER: hierarchical action models for open-world robot manipulation. In *ICLR*, 2025.

Timothy P. Lillicrap, Jonathan J. Hunt, Alexander Pritzel, Nicolas Heess, Tom Erez, Yuval Tassa, David Silver, and Daan Wierstra. Continuous control with deep reinforcement learning. In *ICLR*, 2016.

Yueen Ma, Zixing Song, Yuzheng Zhuang, Jianye Hao, and Irwin King. A survey on vision-language-action models for embodied AI. arXiv:2405.14093, 2024.

Ronald Parr and Stuart Russell. Reinforcement learning with hierarchies of machines. In *NIPS*, pages 1043–1049, 1997.

Edward O Pyzer-Knapp, Jed W Pitera, Peter WJ Staar, Seiji Takeda, Teodoro Laino, Daniel P Sanders, James Sexton, John R Smith, and Alessandro Curioni. Accelerating materials discovery using artificial intelligence, high performance computing and robotics. *npj Computational Materials*, 8(1):84, 2022.

Alec Radford. Improving language understanding by generative pre-training, 2018. OpenAI Blog.

Mayk Caldas Ramos, Christopher J Collison, and Andrew D White. A review of large language models and autonomous agents in chemistry. *Chemical Science*, 16:2514–2572, 2025.

Oleg Sautenkov, Yasheerah Yaqoot, Artem Lykov, Muhammad Ahsan Mustafa, Grik Tadevosyan, Aibek Akhmetkazy, Miguel Altamirano Cabrera, Mikhail Martynov, Sausar Karaf, and Dzmitry Tsetserukou. UAV-VLA: vision-language-action system for large scale aerial mission generation. In *HRI*, pages 1588–1592, 2025.

Mohit Shridhar, Lucas Manuelli, and Dieter Fox. Perceiver-actor: A multi-task transformer for robotic manipulation. In *CoRL*, pages 785–799, 2022.

Ishika Singh, Valts Blukis, Arsalan Mousavian, Ankit Goyal, Danfei Xu, Jonathan Tremblay, Dieter Fox, Jesse Thomason, and Animesh Garg. Progprompt: Generating situated robot task plans using large language models. In *ICRA*, pages 11523–11530, 2023.

Hugo Touvron, Thibaut Lavril, Gautier Izacard, Xavier Martinet, Marie-Anne Lachaux, Timothée Lacroix, Baptiste Rozière, Naman Goyal, Eric Hambro, Faisal Azhar, et al. Llama: Open and efficient foundation language models. arXiv:2302.13971, 2023.

Ziao Wang and Xi Zhu. Enhancing nanocrystal synthesis: A comparative study of online artificial intelligence optimization and offline high-throughput experimentation in chemical material discovery. *ACS Applied Nano Materials*, 7(6):6499–6505, 2024.

Yecheng Wu, Zhuoyang Zhang, Junyu Chen, Haotian Tang, Dacheng Li, Yunhao Fang, Ligeng Zhu, Enze Xie, Hongxu Yin, Li Yi, Song Han, and Yao Lu. VILA-U: a unified foundation model integrating visual understanding and generation. In *ICLR*, 2025.

Jiawen Yu, Hairuo Liu, Qiaojun Yu, Jieji Ren, Ce Hao, Haitong Ding, Guangyu Huang, Guofan Huang, Yan Song, Panpan Cai, Cewu Lu, and Wenqiang Zhang. ForceVLA: Enhancing VLA models with a force-aware moe for contact-rich manipulation. arXiv:2505.22159, 2025.

Rongyu Zhang, Menghang Dong, Yuan Zhang, Liang Heng, Xiaowei Chi, Gaole Dai, Li Du, Dan Wang, Yuan Du, and Shanghang Zhang. MoLe-VLA: Dynamic layer-skipping vision language action model via mixture-of-layers for efficient robot manipulation. arXiv:2503.20384, 2025.

Yicheng Zhao, Jiyun Zhang, Zhengwei Xu, Shijing Sun, Stefan Langner, Noor Titan Putri Hartono, Thomas Heumueller, Yi Hou, Jack Elia, Ning Li, et al. Discovery of temperature-induced stability reversal in perovskites using high-throughput robotic learning. *Nature Communications*, 12(1):2191, 2021.

Qingqing Zhao, Yao Lu, Moo Jin Kim, Zipeng Fu, Zhuoyang Zhang, Yecheng Wu, Zhaoshuo Li, Qianli Ma, Song Han, Chelsea Finn, et al. Cot-vla: Visual chain-of-thought reasoning for vision-language-action models. In *CVPR*, pages 1702–1713, 2025.

Zhehua Zhou, Jiayang Song, Kunpeng Yao, Zhan Shu, and Lei Ma. Isr-llm: Iterative self-refined large language model for long-horizon sequential task planning. In *ICRA*, pages 2081–2088, 2024.

Appendix

A LLM Usage Statement

Large Language Models (LLMs) are used to assist in language polishing and improving the readability of the manuscript.

B Detailed Description of the Self-verification Operations

Subgoal Validation. The LLM is prompted to check whether each subtask aligns with the overall task objective through natural-language self-reflection and identify potential contradictions, redundancies, or omissions.

Constraint Consistency Check. For each subtask, we guide the model to ensure each subtask satisfies key physical, temporal, and causal constraints, detecting invalid ordering (e.g., measuring before synthesis) or mismatches (e.g., heating before reagent addition).

Correction and Refinement. When inconsistencies are identified, the model is prompted to revise and revalidate subtasks until the sequence is logically coherent and operationally feasible.

C Discussion of Why and When Decoupling is Valid

In this section, we provide a brief theoretical analysis of the conditions under which the decoupling between the task-level symbolic planner and downstream execution is valid. We focus on the subtask sequence generated by the task-level planner and analyze its contribution to modularity, while noting that downstream action primitives and RL policies do not affect this argument.

Preliminaries. Let \mathcal{G} denote a high-level task goal, $\mathcal{S} = (s_1, s_2, \dots, s_T)$ the symbolic subtask sequence generated by the task-level planner, and π a low-level execution policy acting on continuous observations $o_{1:T}$. Task success is represented by the event $\mathcal{E} = \{\text{goal achieved}\}$.

Lemma 1 (Task-symbolic sufficiency). *If the execution policy π depends only on observations $o_{1:T}$ given \mathcal{S} , i.e.,*

$$P(\pi | \mathcal{S}, \mathcal{G}, o_{1:T}) = P(\pi | \mathcal{S}, o_{1:T}),$$

then the goal \mathcal{G} influences execution only through the symbolic plan \mathcal{S} .

Lemma 2 (Conditional independence). *If symbolic decompositions and observations are conditionally independent given the goal,*

$$P(\mathcal{S}, o_{1:T} | \mathcal{G}) = P(\mathcal{S} | \mathcal{G}) P(o_{1:T} | \mathcal{G}),$$

then \mathcal{S} carries no redundant information about $o_{1:T}$ beyond \mathcal{G} .

Proposition 1 (Factorization of success probability). *Under Lemmas 1 and 2, the probability of success can be factorized*

as

$$\mathcal{E} := \max P(\pi | \mathcal{G}, o_{1:T}), \quad (8)$$

$$P(\pi | \mathcal{G}, o_{1:T}) = \sum_{\mathcal{S}} P(\pi, \mathcal{S} | \mathcal{G}, o_{1:T}) \quad (9)$$

$$= \sum_{\mathcal{S}} P(\pi | \mathcal{S}, o_{1:T}) P(\mathcal{S} | \mathcal{G}). \quad (10)$$

Hence the contribution of reasoning (via $P(\mathcal{S} | \mathcal{G})$) is decoupled from perception and control (via $P(\mathcal{E} | \mathcal{S}, o_{1:T})$).

This shows that improvements in task-level reasoning and low-level execution independently contribute to overall success, consistent with modular planning frameworks [Kaelbling *et al.*, 1998].

When decoupling is valid. Decoupling holds if:

- Each subtask s_i contains sufficient symbolic information for execution without direct dependence on \mathcal{G} ;
- Observations and subtasks are approximately conditionally independent given \mathcal{G} ;
- Subtasks capture the causal structure of the task relevant for achieving the goal.

For example, for a task like “mix reagents A and B”, the task-level planner may output subtasks such as *add reagent A* and *add reagent B*. Each subtask carries enough symbolic information for downstream execution, the low-level observations for executing these actions are largely independent of the high-level goal, and the sequence preserves the necessary causal order. Compared to a fully end-to-end approach that maps from goal and observations directly to actions, decoupling reduces the complexity and naturally aligns with the modular structure of the task.

Overall, while the conditions are not guaranteed in all settings, they are relatively easy to satisfy in well-structured tasks, which explains why decoupling is a practical and effective design choice.

When decoupling may fail. In practice, these assumptions may be violated in cases such as:

- If \mathcal{S} omits crucial physical requirements (e.g., exact forces or contact stability), then $P(\mathcal{E} | \mathcal{S}, o_{1:T})$ still implicitly depends on \mathcal{G} .
- If \mathcal{S} is entangled with perception (e.g., symbolic labels directly derived from raw visual embeddings), then independence may fail.
- If success depends on hidden histories not captured in \mathcal{S} , factorization does not hold.

Fallback as constrained refinement. Execution failures can be modeled as the discovery of additional constraints C on symbolic decompositions. Formally,

$$\mathcal{S}^{(k+1)} \sim P(\mathcal{S}^{(k)} | \mathcal{G}, C),$$

where C is induced from observed failure conditions (e.g., contact instability). If the constraint set C is finite and each refinement step reduces the feasible set of \mathcal{S} , then iterative fallback converges in at most $|C|$ iterations: either a feasible \mathcal{S}^* is found, or infeasibility is proven. This parallels refinement strategies in symbolic AI.

Limitations and outlook. Our current system does not implement fallback at this stage, i.e., the planner runs only once. Nonetheless, the above analysis suggests a principled extension: failed executions could be recycled as symbolic constraints to refine subtask decomposition. Future work may explore this integration, which would tighten the link between symbolic reasoning and embodied feedback while preserving modularity.

D Training Details

We implemented our multimodal predictor using PyTorch. The backbone of the diffusion model is U-Net. The multimodal predictor is conducted with the following configuration:

- Number of diffusion steps: 100
- Sampling steps: 100
- loss: L2
- SNR-based loss weighting: True
- Image size: (256, 256)

We adopt OpenAI’s CLIP as the text encoder, with its parameters kept frozen throughout training to preserve the pre-trained semantic representations. The multimodal predictor is trained on an NVIDIA RTX 4090 GPU, and the model checkpoints are saved every 2,500 iterations. The training is conducted with the following configuration:

- Learning rate: 1e-5
- Batch size: 1
- Image sequence length: 8
- Total training steps: 60,000
- Precision: Mixed precision (fp16)

The training process of multimodal predictor takes approximately three days on our collected dataset.

E Results of Different Large Models

Since only relying on large language models to evaluate outputs can be inaccurate, which often leading to redundant content. Thus we assessed the performance of different LLMs and VLMs on our defined tasks through human evaluation. For each model, we prompt the large model to generate 25 task decompositions in each round, and compute the corresponding success rate based on expert evaluations. The final success rate reported in the table is the average of 3 rounds. We use LLaMA3.1 as the LLM and GPT-4o as the VLM in our framework.

Table 5: Success rate (%) of different LLMs

Model	Pick_place	Pour	Stir	Mix	Crystallize
Qwen3	45.2	36.0	100.0	88.0	56.0
Deepseek-V3	98.4	44.0	100.0	33.2	90.4
LLama3.1 (ours)	100.0	74.4	100.0	73.2	76.0

Table 6: Success rate (%) of different VLMs

Model	Pick_place	Pour	Stir	Mix	Crystallize
Qwen2.5	77.2	76.0	76.0	73.2	72.0
Llama3.2	82.4	80.0	82.4	78.4	76.0
GPT-4o (ours)	100.0	100.0	100.0	98.4	98.4

F Task Details

Our collected dataset includes five task types defined in simulation: Pick_place, Pour, Stir, Mix, and Crystallize, as well as two real-world-only tasks: Weigh and Shake. To support these tasks, we define four action primitives: move, grasp, pour, and stir, which capture core operations commonly involved in scientific experimental procedures. All visual data are collected at a resolution of 512×512 .

- **Pick_place:** The pick_place task includes 3 types of object manipulation tasks: moving the cuboid to the beaker, moving the cuboid to the glass garden, and moving the cylinder to the beaker. In these tasks, we use cuboids and cylinders to represent objects with different shapes and graspable properties. Fig. 12 illustrates example images from the pick_place task.
- **Pour:** Considering the specific procedural requirements of certain scientific experiments, we collected a visual demonstration set for the pour task. We use cups as the manipulable object to represent the action of pouring. The execution of the pour operation requires prior completion of the move and grasp operations from the pick_place task.
- **Stir:** The stir task is designed to perform liquid stirring operations. A thin rectangular block is used as a graspable stirrer to ensure the successful execution of the stir operation. Similar to pour, the stir operation also requires prior completion of the move and grasp operations.
- **Mix:** Mix is a longer-horizon task. Considering the frequent use of reactant mixing in scientific experiments, we incorporate this task into our setup. This long-horizon task can be decomposed and accomplished through a combination of the three previously defined action primitives.
- **Crystallize:** The crystallize task has a similar horizon length to the mix task, both being more complex than the former 3 tasks. This task can also be decomposed into a sequence of our designed action primitives. Unlike the mix task, however, the crystallize task requires more frequent use of pick_place operations rather than pour.
- **Weigh:** The weigh task is a real-world-only task that measures the weight of a container using a laboratory balance. Due to the difficulty of accurately modeling specific instruments in simulation, this task is executed directly in the real environment and relies on visual feedback to complete the weighing procedure.

Table 7: Success rate (%) of CoT reasoning and its ablations (w/o Step1–4)

Task	CoT	CoT w/o Step1	CoT w/o Step2	CoT w/o Step3	CoT w/o Step4
Pick_place	100.0	44.0	37.2	46.4	41.2
Pour	74.4	13.2	22.4	25.2	22.4
Stir	100.0	57.2	29.2	78.4	61.2
Mix	73.2	40.0	25.2	66.4	13.2
Crystallize	76.0	70.4	49.2	54.4	30.4

- **Shake:** The shake task is another real-world-only task, where a container is placed onto a laboratory shaker to perform mixing through shaking. Similar to weigh, this task is executed without a corresponding simulation environment and is realized through a sequence of predefined action primitives.

G CoT Prompt design

Our CoT reasoning of the LLM is designed in 4 steps. Each step guides the LLM to think through how to properly decompose the long-horizon task and evaluate whether the resulting short-horizon subtasks are sufficient to accomplish the original objective. This decomposition process does not require visual input.

Instead, the model relies on commonsense reasoning, following the structured CoT prompts to complete the task breakdown. The complete reasoning chain is illustrated in Fig. 8a.

We also conducted distillation experiments on each of the four stages to demonstrate that they are essential components in the task decomposition process. The success rate is evaluated in the same manner as the section of “Results of Different Large Models”.

We evaluated the task decomposition success rate of CoT reasoning when each module is ablated. The result is shown in Table 7.

Meanwhile, we defined two common types of errors for analysis: Step Redundant Error (E1) and Step Logical Error (E2), allowing for a more detailed evaluation of decomposition quality. We further record the occurrences of two defined error types, which are shown in Table 8. We use the crystallization cultivation experiment as an example to illustrate the two error types: E1 and E2.

The correct CoT module output for the crystallization cultivation experiment is shown in Fig. 7a. We also provide example output images illustrating E1 and E2 errors, which are shown in Figs. 7b and 7c. In the E1 example, the model repeatedly outputs the instruction “pick up cuboid”. Although the overall sequence is structurally complete, the redundancy in a single step leads to its classification as an E1 error. In the E2 example, the model outputs “pour contents from cuboid” when there is no object inside the cuboid. This results in a logically incorrect step, thus leading to its classification as an E2 error.

H Efficiency Validation

This appendix provides supplementary validation experiments on the efficiency of CAPER under reduced multimodal predictor resolution. While all main experiments are conducted with an MP input resolution of 256×256 , we retrain the MP at a lower resolution to evaluate the feasibility of accelerating execution (Table 9).

We retrain the multimodal predictor with an input resolution reduced from 256×256 to 128×128 , while keeping all other components unchanged. In particular, the task-level planner, VLM, and low-level RL controller are directly reused without retraining. We evaluate the retrained MP on the long-horizon tasks Mixing and Crystallize. Results show only minor differences in success rates compared to the original resolution, indicating that the procedural structure and execution policies of CAPER are robust to changes in visual prediction fidelity.

Under the reduced resolution setting, we further explore an optional strategy that provides newly observed images to the MP during execution to reduce error accumulation. This strategy yields a modest improvement in success rates on long-horizon tasks. However, due to the inference latency of the MP, the overall gain remains limited. As a result, online visual updates are not enabled in the main experiments.

I VLM Prompt design

The prompt design for the VLM is primarily aimed at mapping the subtask instructions generated by the large language model to our predefined three action primitives, in order to guide the robot’s motion accordingly. The detailed prompt structure is illustrated in Fig. 8b.

J Experiment in real-world scenario

We replicate the experimental setup from the simulation environment in a real-world setting and evaluate the success rate using our proposed method. We present the experimental images of real-world scenario in tasks such as Pick_place, as shown in Fig. 9 - 22. Notably, our framework allows flexible task skipping based on real-time conditions. In the weigh task, when the beaker is already on the balance, CAPER can bypass this subtask without additional actions. We additionally analyze common sim-to-real failure cases in Figs. 19 and 22. In the first case, the robot collides with an unseen object because the detector fails to recognize it. This object has not been included in our YOLOv8 fine-tuning set, leading to a missing detection and an incorrect motion plan. In the second

Table 8: Error rates (%) of E1 and E2 under CoT reasoning and its ablations (w/o Step1–4)

Task	CoT		CoT w/o Step1		CoT w/o Step2		CoT w/o Step3		CoT w/o Step4	
	E1	E2	E1	E2	E1	E2	E1	E2	E1	E2
Pick_place	0.0	0.0	54.4	26.4	62.4	10.4	42.4	30.4	58.4	20.0
Pour	2.6	25.6	86.4	18.4	76.0	9.2	70.4	34.4	77.2	30.4
Stir	0.0	0.0	42.4	25.2	66.4	34.4	14.4	6.4	39.8	0.0
Mix	8.0	26.8	56.0	46.4	10.4	76.0	9.2	33.2	0.0	86.8
Crystallize	10.0	14.0	0.0	29.6	18.4	38.4	6.4	34.4	20.0	69.2

1. Pick up cuboid (pick_and_place) → Logical purpose: Prepare for placing in beaker
2. Place cuboid in beaker (pick_and_place) → Logical purpose: Ensure cuboid is in the beaker
3. Pick up cup (pick_and_place) → Logical purpose: Prepare for pouring
4. Pour contents from cup into beaker (pour) → Logical purpose: Transfer liquid to beaker
5. Pick up stir stick (pick_and_place) → Logical purpose: Prepare for stirring
6. Stir the liquid (stir) → Logical purpose: Finish the task

(a) Correct CoT output

"1. Pick up cuboid (pick_and_place) → Logical purpose: Prepare for placing near the beaker
 2. Place cuboid near the beaker (pick_and_place) → Logical purpose: Position for future use
 3. Pick up cup (pick_and_place) → Logical purpose: Prepare for pouring
 4. Pour contents from cup into beaker (pour) → Logical purpose: Transfer experimental liquid
 5. Pick up cuboid (pick_and_place) → Logical purpose: Prepare for grasping and moving
 6. Pick up stir stick (pick_and_place) → Logical purpose: Prepare for stirring
 7. Place cuboid on stir stick (pick_and_place) → Logical purpose: Secure the cuboid for stirring"

(b) E1 error example: redundant step

"1. Pick up cuboid (pick_and_place) → Logical purpose: Prepare for movement
 2. Move cuboid to the beaker (slant) → Logical purpose: Position cuboid for subsequent steps
 3. Pick up cuboid (pick_and_place) → Logical purpose: Prepare for pouring
 4. Pour contents from cuboid into the beaker (pour) → Logical purpose: Prepare for stir
 5. Pick up stir stick (pick_and_place) → Logical purpose: Prepare for stirring
 6. Stir the liquid (stir) → Logical purpose: Finish the task"

(c) E2 error example: incorrect logic

Figure 7: Examples of CoT module outputs: (a) correct, (b) E1 error, (c) E2 error.

case, the robot fails to grasp the target object due to inaccurate depth-based localization from the D415 sensor, resulting in insufficient gripper contact during execution.

Setting	Mixing	Crystallize
MP (256 × 256)	52.3	30.1
MP (128 × 128)	51.6	29.8
MP (128 × 128) (online)	55.2	30.6

Table 9: Validation of reduced MP resolution and online visual updates on long-horizon tasks.

```

## Task: "{question}"
Environment Rules (Important Constraints):
- The cup contains the liquid, which needs to be Poured in the beaker.
- The Cuboid is the solid of the experiment, which only can Pick_and_place.
- The beaker is immovable and ungraspable.
- The Stir operation requires to grasp the stick.
## Flow of Thought Reasoning:
Step 1: Understand the task objective Thinking: What is the final goal we need to achieve? What would constitute success?
Step 2: Identify logical prerequisites Thinking: What must be true before we start? What objects must exist and what are the constraints we must obey?
Step 3: Decompose into primitive operations Thinking: What sequence of basic operations (pick_and_place, pour, stir, slant) would accomplish this task? **while strictly following all environment rules**
Step 4: Validate the operation sequence Thinking: Is this sequence logically complete and compliant with the constraints? Would it successfully accomplish the task?
## Final Output Format: Only output the operation sequence using this format: 1. [First operation] → Logical purpose: [Why this step is necessary] 2. [Second operation] → Logical purpose: [Why this step is necessary] ... n. [Final operation] → Final outcome: [How this completes the task] Be sure not to include any actions that grasp or move the beaker. Use only legal, necessary operations under the constraints Example 1: Mixing solutions from two beakers Task: Mix solutions from two beakers on the table. Chain-of-thought analysis: Step 1: Understand the task objective Thinking: The goal is to combine the contents of two beakers to create a mixed solution. Success means having all liquid combined in one container. Step 2: Identify logical prerequisites Thinking: We must have two beakers containing solutions. They must be accessible for manipulation. Step 3: Decompose into primitive operations Thinking: Logically, we need to move one solution into the other, then ensure they're properly mixed. This requires picking up one beaker, pouring its contents into the other, and then stirring. Step 4: Validate the operation sequence Thinking: This sequence covers all necessary steps: transferring the liquid and ensuring proper mixing. The task would be successfully completed. Operation sequence: 1. Pick up cup (pick_and_place) → Logical purpose: Prepare for pouring 2. Pour contents in the beaker(pour) → Logical purpose: Prepare for stirring 3. Pick up one cup (pick_and_place) → Logical purpose: Prepare for pouring 4. Pour contents in the beaker(pour) → Logical purpose: Prepare for stirring 5. Stir the liquid (Stir) → Logical purpose: Finish the task. Only give the Operation sequence.

```

(a) Design of the CoT prompt

You are given:

1. The LLM's initial task decomposition
2. The target task
3. Left image = global environment, right image = target state. The LLM's output may contain logical or procedural errors.

Your job:

1. Correct the decomposition so it is logically valid.
2. Break each step into the only primitive actions: Move, Grasp, Slant, Stir.
3. Use the following special rules: - pick_and_place → ["Move to <Object> and grasp 0", "Move to <Object> and grasp 1"], - Pour → ["Move to <Object> and grasp 0", "Slant", "Place on the desk"], - Stir → ["Move to Stick and grasp 0", "Stir"]
4. Output only a Python list of actions.

Environment Rules(Important Constraints):

- The beaker is immovable and ungraspable.
- The cup contains the liquid, which need to slant in the beaker.
- The cuboid represents the solid of the experimental, which only can move and grasp.
- The stirring operation requires grasping a stir stick.

Example 1: Task: Move the cuboid to the beaker. LLM: 1. Pick up cuboid (pick_and_place) → Logical purpose: Prepare for placing in beaker 2. Place cuboid in beaker (pick_and_place) → Logical purpose: Finish the task. Output should be: ["Move to the cuboid and grasp 0", "Move to the beaker and grasp 1"].

Example 2: Task: Pour the liquid. LLM: 1. Pick up cup (pick_and_place) → Logical purpose: Prepare for pouring 2. Pour the liquid to the beaker → Logical purpose: Finish the task. Output should be: ["Move to the cup and grasp 0", "Move to the beaker", "Slant"].

The LLM's initial task decomposition: "{{lm}}". The target task: "{{task}}". Give the output. Remember the environment rules. The output should be merge into a single list. Reduce the length.

(b) Design of the VLM prompt

Figure 8: Prompt designs for different reasoning strategies: (a) CoT and (b) VLM.

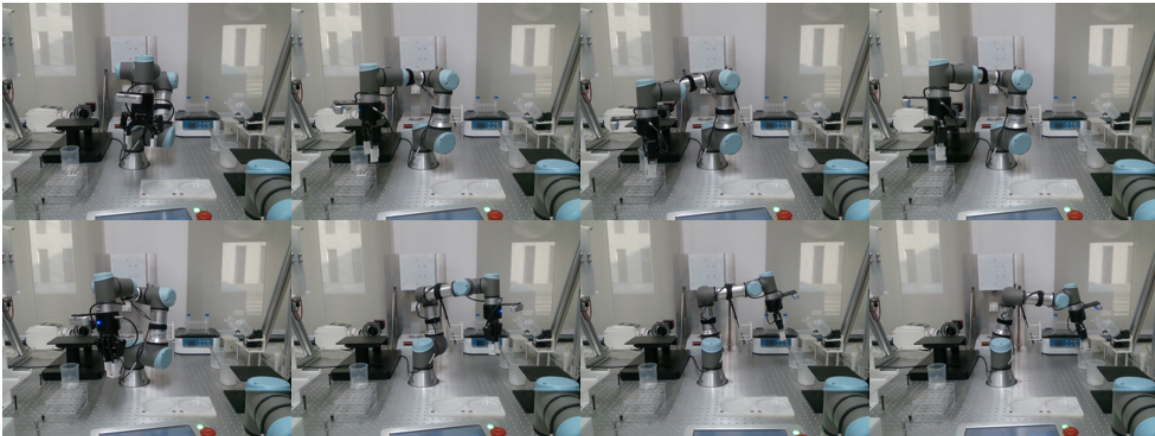


Figure 9: "Pick_place" task in real-world scenario.



Figure 10: “Crystallize” task in real-world scenario.

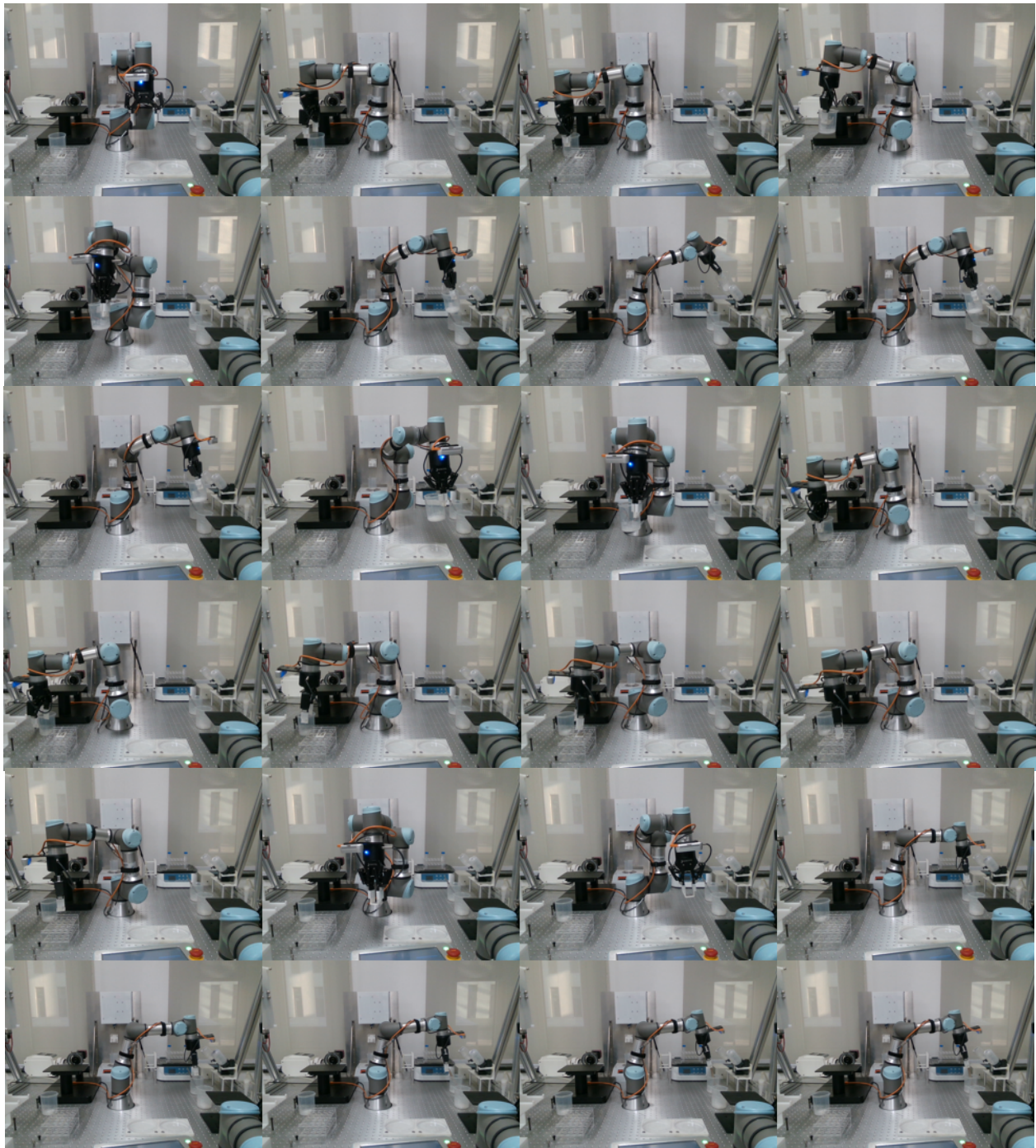


Figure 11: “Mix” task in real-world scenario.

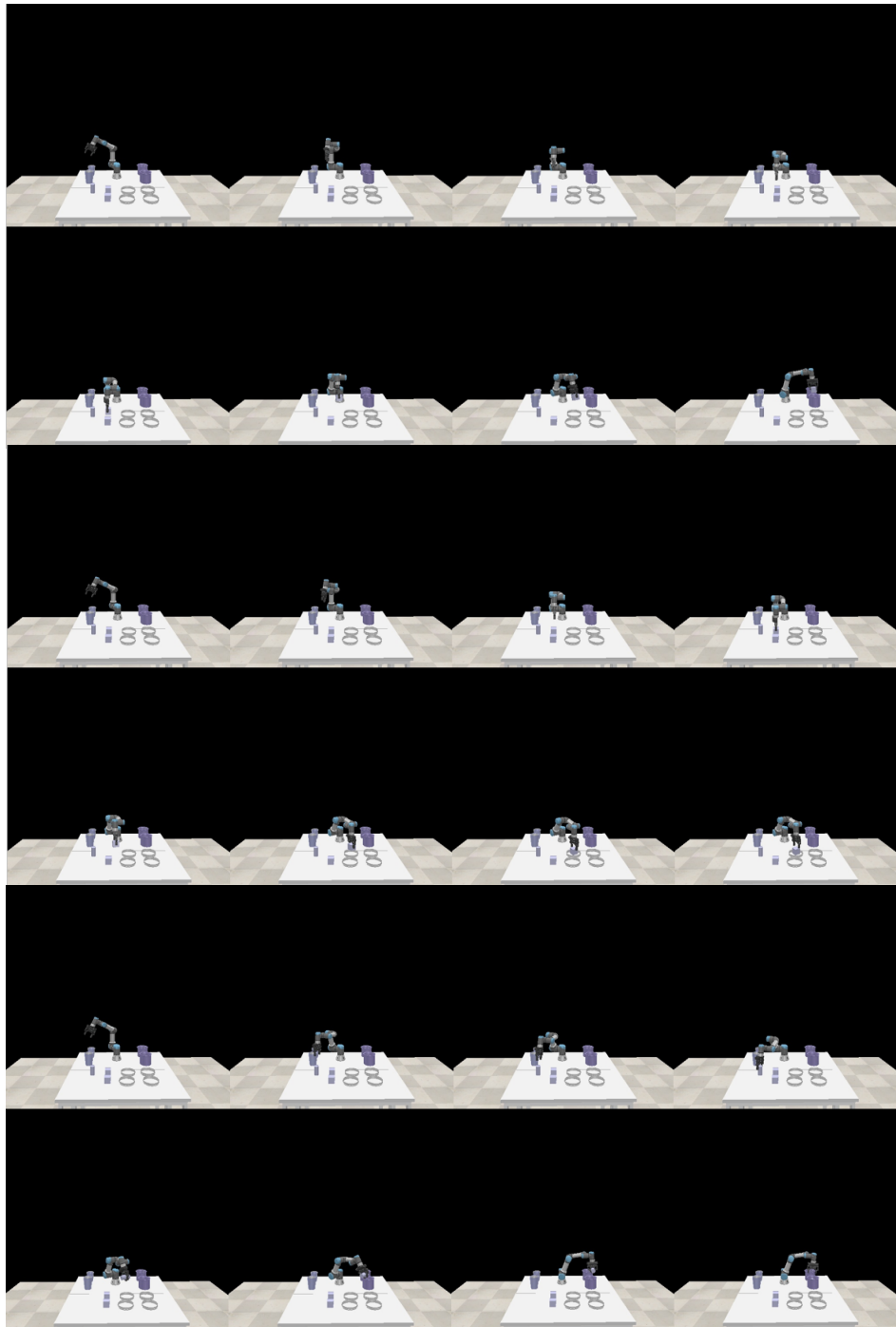


Figure 12: Visualization of the “pick_place” task.

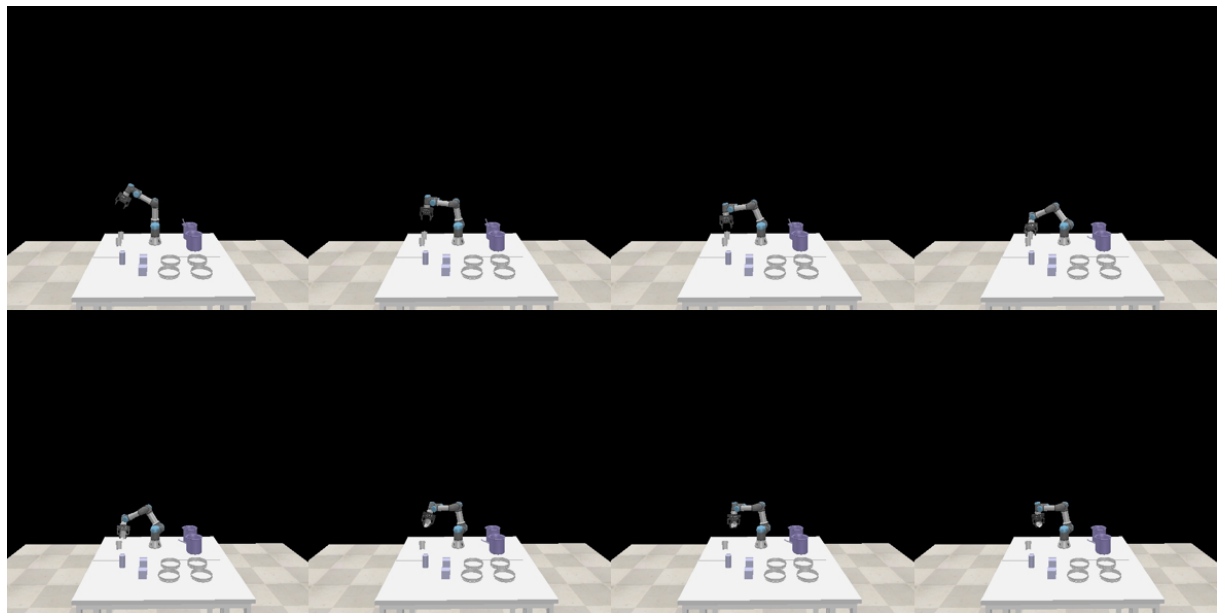


Figure 13: Visualization of the “pour” task.

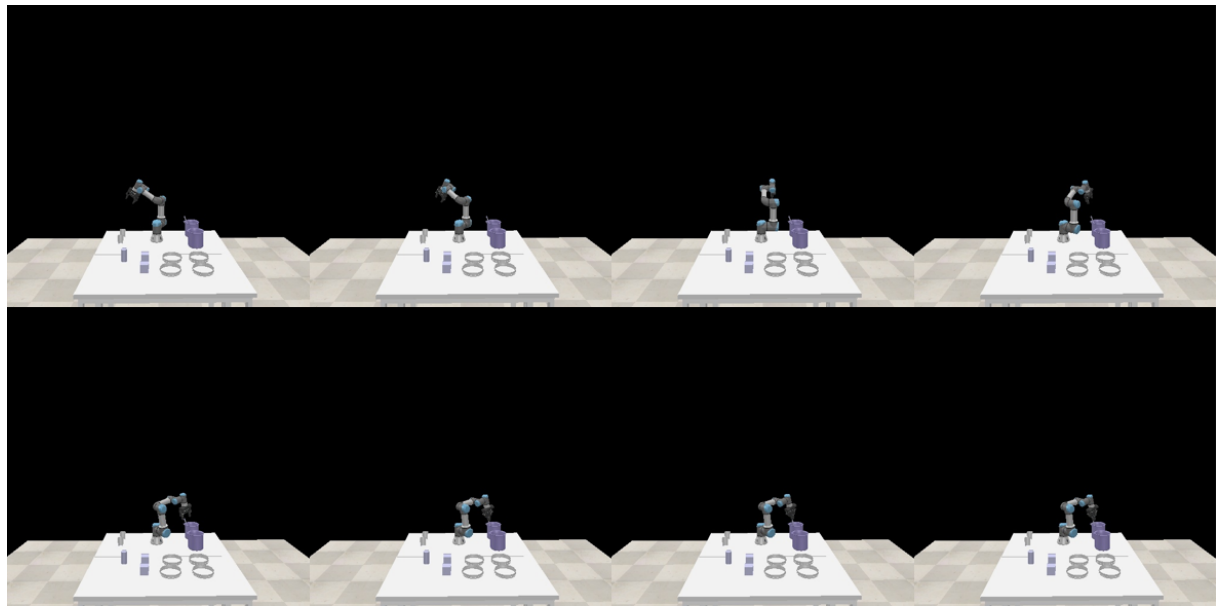


Figure 14: Visualization of the “stir” task.

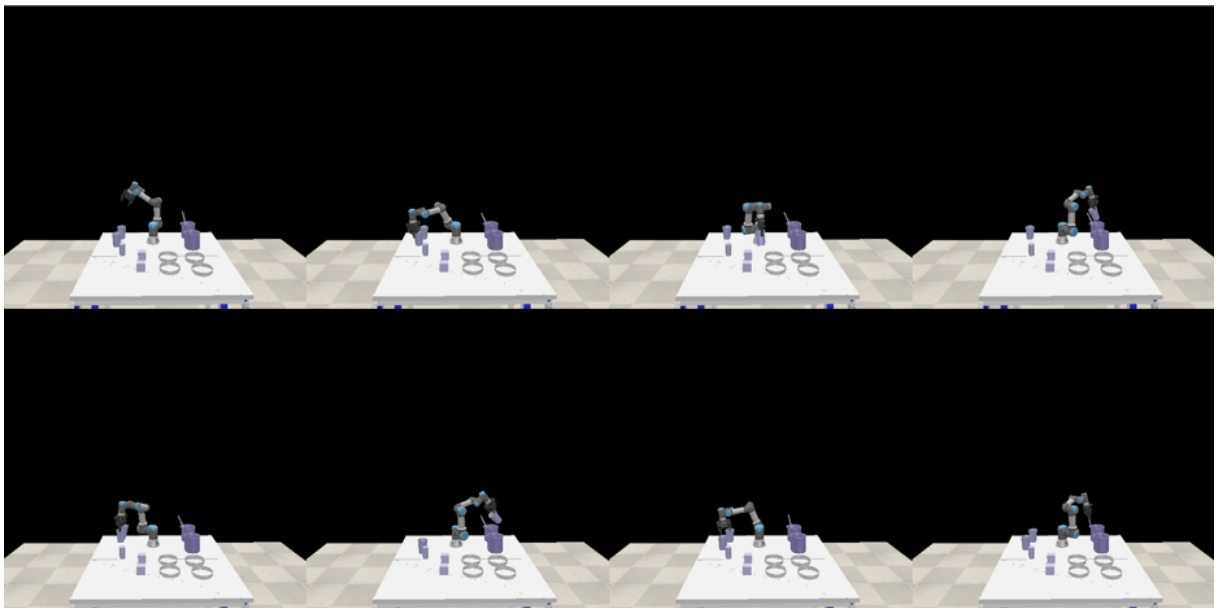


Figure 15: Visualization of the “mix” task.

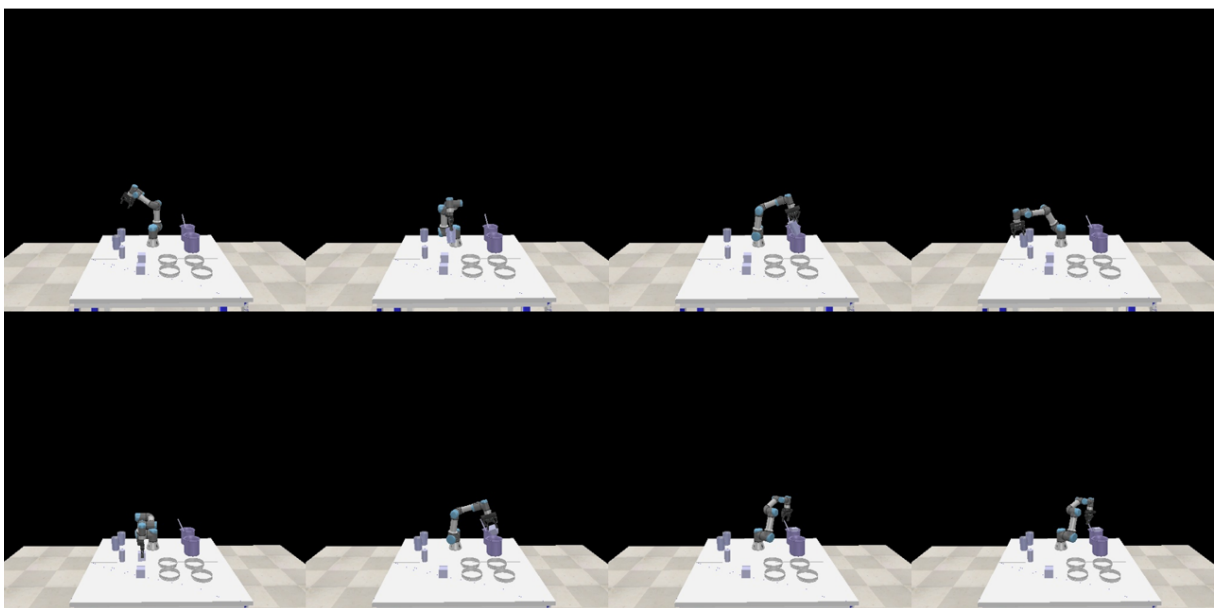


Figure 16: Visualization of the “crystallize” task.



Figure 17: Human demonstration of the “weigh” task in real-world scenario.

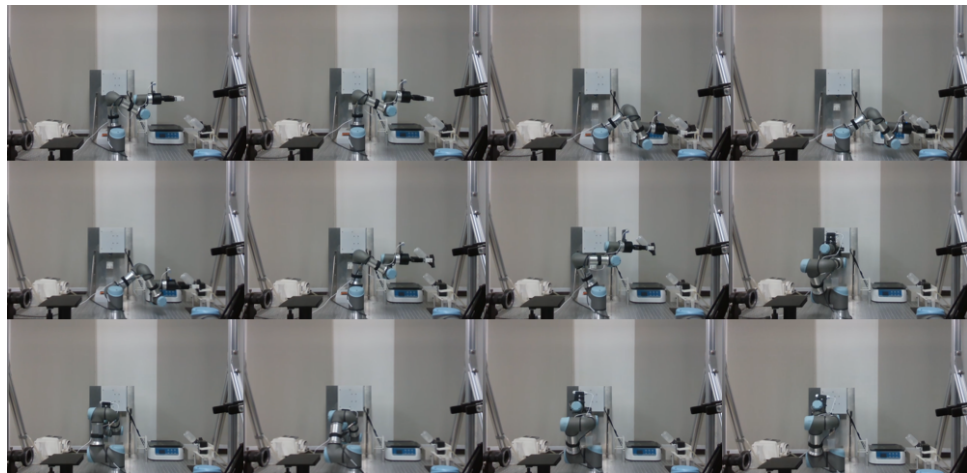


Figure 18: “Weigh” task in real-world scenario.

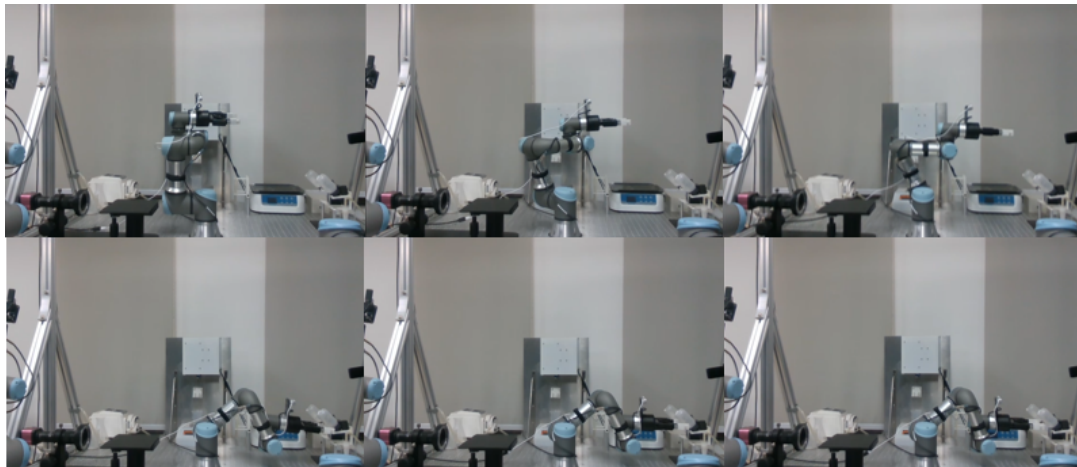


Figure 19: Failure case of the “weigh” task in real-world scenario.

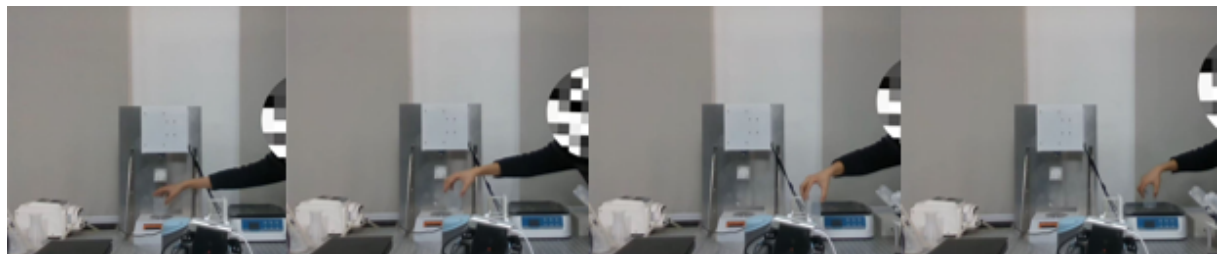


Figure 20: Human demonstration of the “shake” task in real-world scenario.

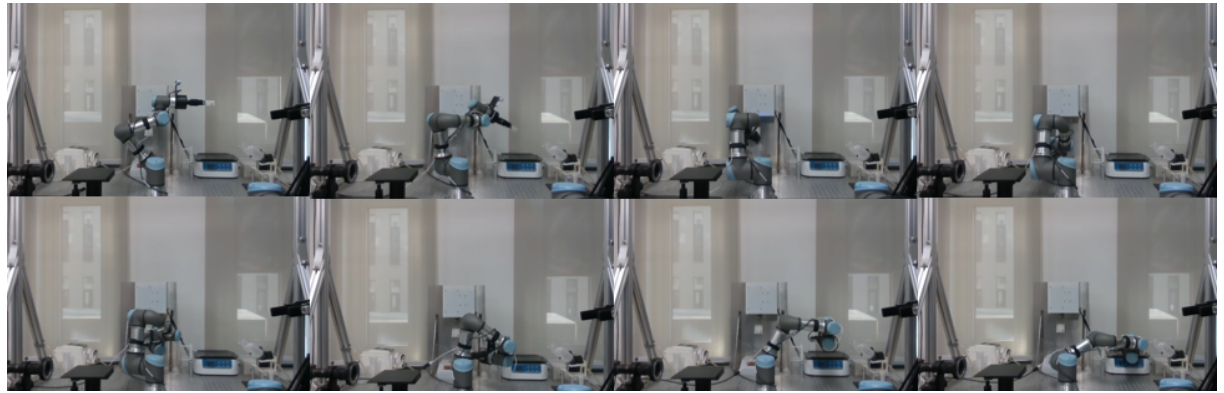


Figure 21: “Shake” task in real-world scenario.

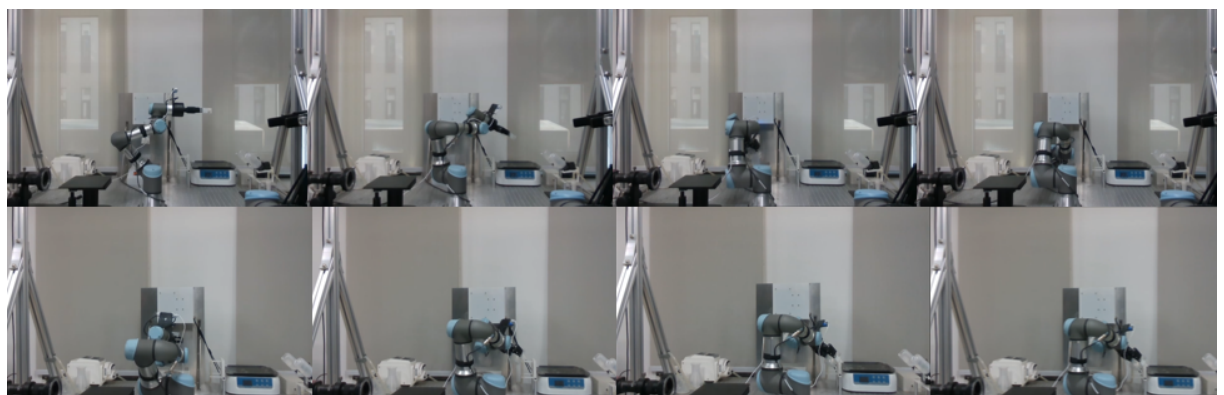


Figure 22: Failure case of the “shake” task in real-world scenario.